Storm-Substorm Relationships During the 4 October, 2000 Storm. IMAGE Global ENA Imaging Results

Pontus C:son Brandt, Donald G. Mitchell, Shin Ohtani, Robert Demajistre, Edmond C. Roelof

The Johns Hopkins University Applied Physics Laboratory, Laurel, Maryland

Jörg-Micha Jahn, Craig Pollock

Southwest Research Institute, San Antonio, Texas

Geoff Reeves

Los Alamos National Laboratories, Los Alamos, New Mexico

Global ion distributions in the 1-200 keV energy range from the main phase of the geomagnetic storm on 4 October 2000 are presented and analyzed. Proton distributions have been obtained by inverting energetic neutral atom (ENA) images from the high energy neutral atom (HENA) instrument on board the IMAGE satellite using a constrained linear inversion technique. The storm is characterized by a 24-hour long main phase where the IMF B_z steadily decreases followed by a 2 day recovery. Several substorms occured during the main phase as can be seen from in-situ measurements from geosynchronous satellites (LANL, GOES). Substorm injections during the early main phase, when the dawn to dusk electric field was weak, ocurred on closed trajectories. A strong asymmetric ring current developed as the IMF B_z decreased gradually to about -10 nT. A substorm ocurred at about 17:30 UT which injected plasma onto open trajectories with no clear change in the morphology of the partial ring current. As the IMF B_z increased towards zero, substorms were observed to inject ions onto closed trajectories. The peak of the ring current moved from L=5 to L=3 during the entire main phase. A preliminary inspection of $\sim$80-160 keV oxygen ENA fluxes reveal a one order of magnitude increase during the entire main phase, implying that O^+ contributed significantly to this storm. Rapid decrease followed by decay ($\sim$1 h) was superposed on the gradual increase of the oxygen ENA. Each one of these "bursts" are associated with a substorm onset. No burst-like features were present in the hydrogen data. In order to quantify the variations in the ring current energy content, the equivalent magnetic disturbance D_{ENA} is calculated for the L$\leq$6 proton distributions using the Dessler-Parker-Sckopke relation. Our calculated D_{ENA} suggests that substorm proton injections did not increase the ring current energy content over the main phase. Together with the fact that the proton ring current was mostly partial, this shows that the dominant ring current energy increase must have been due to increased convection. However, the long-term increase in oxygen ENA fluxes suggests that O^+ may have been continuously extracted from the ionosphere throughout the main phase and subsequently energized at each substorm dipolarization to give rise to the oxygen ENA bursts. We also discuss implications of strong electric fields in the inner region L$<$4.

1. INTRODUCTION

Historically it was believed that a geomagnetic storm was the effect of many substorms [*Akasofu*, 1968]. It was later recognized by *Gonzalez and Tsurutani* [1987] that the requirement for a geomagnetic storm to occurr was an IMF $B_z \leq$-10 nT for at least 3 h. More recent studies have shown that convection is the dominant driver in geomagnetic storms and that the main-phase ring current is mostly partial where ions drift on open trajectories out through the dayside magnetopause [*Liemohn et al.*, 2001]. However, there still remains a question of how much the substorm injections during a storm main phase contribute to the overall storm time energy content of the ring current.

The problem we investigate in this paper can be summarized as follows. The storm intensity has been characterized by the D_{st}, and more recently, by the SYM-H and ASY-H indices. These are indices directly calculated from the magnetic disturbance measured at the equatorial surface. The magnetic disturbance can be related to the total energy content of the ions that flow around the Earth, via the Dessler-Parker-Sckopke (DPS) relation [*Dessler and Parker*, 1959; *Sckopke*, 1966]. Now the problem is how much of the growth of the energy content during a geomagnetic storm can be attributed to substorms and how much can be attributed to an increase in the overall convection strength. Once plasma is injected during a substorm onto open trajectories it will not contribute further to the overall growth of the energy. This is because the injected particles will be lost through the magnetopause. So, the only way accumulated substorm injections can contribute to the overall growth is if the injections are onto closed drift trajectories.

On the other hand, the energy content of plasma being transported by the $\mathbf{E} \times \mathbf{B}$ (in other words, the partial ring current) can increase if the cross-tail (convectional) electric field increases. The reason for this is that a stronger cross tail electric field makes the tranport of particles be dominated by the $\mathbf{E} \times \mathbf{B}$ drift closer to Earth and so open trajectories are allowed closer to Earth. Another way of saying this is that the Alfven boundary (boundary between open and closed trajectories for particles with given magnetic moment) shrinks for higher cross tail electric field. This will in turn lead to adiabatic energization since the plasma is now transported into a region with higher magnetic field strength, and thus the energy content of the partial ring current will increase.

Since the IMF B_z decreases during a main phase of a storm, the convectional electric field increases and the location of the innermost open trajectory grows closer to Earth. Therefore, plasma cannot be trapped during the main phase of the storm. However, depending on how fast the convectional electric field turns off (the start of storm recovery phase) more or less plasma will be trapped. Thus, if the con-

vectional electric field increases monotonically, any trapped population during a storm main phase could only come from substorm injections. We will examine the global ion distribution during such periods and investigate how much of the growth of the total energy is due to substorms injections or increased convection.

In this paper we will present ENA images from the main phase of the 4 October 2000 storm. The ENA images have been inverted to obtain an equatorial proton distribution, using a constrained linear inversion technique. In order to quantify how much the substorm injections contribute to the overall storm growth we compute the equivalent magnetic disturbance D_{ENA} for the global proton distributions during the main phase. By looking at the local time distribution of the obtained global proton distribution at a given energy we can infer if those protons are on closed or open trajectories. The contribution of those protons to the D_{ENA} relative to other energies will tell us how much it contributes to the over all growth of the total energy of the main-phase ring current. In addition to this we will discuss how the oxygen ENA flux increased over the main phase. We also discuss briefly the spectral features of the main phase indicating that there was a deep potential minimum on L$\leq$3 implying a significant electric fields. We compare our results to a model derived electric field by *Ridley and Liemohn* [2002]. The purpose of this study is to investigate what restrictions can be put on different energy sources to the ring current energization by analyzing the global ion distributions we have obtained.

2. INVERSION TECHNIQUE

We use a constrained linear inversion technique that closely follows the method described by *Twomey* [1977] and also similar to *Perez et al.* [2001]. Previous studies [*Henderson et al.*, 1997; *C:son Brandt et al.*, 2001] have used a forward modeling technique based on a parametrized model of the ion distribution developed by *Roelof and Skinner* [2000]. This inversion technique was described in *C:son Brandt et al.* [2002a] and we only outline its main components here. The idea is to expand the line of sight (LOS) integral that describes the production of ENAs into sums of linear quadrature and then equating them with the observed image and in that way determine the quadrature coefficients. In the present formulation the pitch angle distribution (PAD) is described by one isotropic component and one linear component representing the field aligned and perpendicular shape of the PAD. In this paper we focus only on the isotropic component. The ion distributions were clamped down to zero at L=2 and L=16. We use here the day-midnight asymmetric exosphere based on the DE-1 measurements reported by *Rairden et al.* [1986] and also used by [*C:son Brandt et al.*,

2002a]. The absolute fluxes obtained by our algorithm appear to be somewhat overestimated. The calculated D_{ENA} calculated below should therefore not be taken as absolute, but rather as a relative indicator on the total energy content of the ring current. Fluxes should be correct in a relative sense.

3. CALCULATING MAGNETIC DISTURBANCE

We use the retrieved ion distributions to calculate the magnetic disturbance at the equator on the surface of the Earth. We do this by using the Dessler-Parker-Sckopke (DPS) relation [*Dessler and Parker*, 1959; *Sckopke*, 1966], which states that the horisontal magnetic perturbation ΔB at the equator can be written

$$\Delta B = -\frac{2}{3}\frac{E_{tot}}{E_m}B_0, \tag{1}$$

where B_0 is the nominal dipole magnetic field intensity at the surface. The magnetic energy E_m contained in the dipole magnetic field and can be written

$$E_m = \frac{4\pi}{3\mu_0}B_0^2 R_E^3. \tag{2}$$

The total energy of the particles E_{tot} is expressed as the volume integral over the energy density. Note that the magnetic disturbance at Earth as expressed in Equation (1) is independent of L. We can obtain the energy density ϵ by

$$\epsilon = 4\pi \int p^2 f(p) E dp, \tag{3}$$

where E is the energy of the ions and m is the ion mass, where we have assumed protons. $p = mv$ is the momentum of the ions. The distribution function f (in momentum space) can be related to the ion flux (differential in energy) through

$$j(E) = p^2 f(p). \tag{4}$$

Transforming integral (3) to sums for an isotropic pitch angle distribution in ϕ and L space we can write Equation (1) to a first approximation

$$D_{ENA} \approx -\frac{64}{35}\frac{\mu_0 m^2}{B_0}\sum_{ijk} J_{ijk}\frac{E_i^2 L_j^2}{(2mE_i)^{\frac{3}{2}}}\Delta L_j \Delta\phi_k, \tag{5}$$

where μ_0 is the magnetic permeability in vacuum, J_{ijk} is the proton flux (cm^{-2} sr^{-1} s^{-1}) at energy E_i in a finite interval ΔE_i, L-shell L_j and local time angle ϕ_k. The bin size in L and ϕ is denoted ΔL and $\Delta\phi$. The approximation comes from the fact that we have neglected the L-dependence in our evaluation of the flux tube volumes. The error is about 20% at L$\leq$3, but rapidly decreases as L increases. We will use this formula to calculate the magnetic disturbance from the

proton distributions. Since the DPS relation assumes a pure dipole field we will only calculate it for ion distributions on L≤6.

4. GLOBAL STORM OBSERVATIONS

The 4 October storm main phase was characterized by a long and gradual decrease of the IMF B_z. It ended by some rapid fluctuations in the IMF and then a gradual recovery. About a half a dozen substorms ocurred during 4 October that showed up clearly in the Los Alamos National Laboratory (LANL) geosynchronous proton data as well as in the geomagnetic field components observed by the GOES satellite. We will only show ENA data from two of those substorms here. *C:son Brandt et al.* [2002a] have examined ENA and in-situ data from some of these substorm in more detail.

Plate 1 shows the SYMH (black line) and (negative) ASYH (green line) for the main phase we are studying in this paper. The red line is the electric field E_y set up by the solar wind ($v_x B_z$). Note that the E_y increases up until approximately 18:00 UT and then starts slowly decreasing. This indicates that the Earthward $\mathbf{E} \times \mathbf{B}$ drift feeds more and more plasma into the nightside magnetosphere and that the Alfven layer (for given magnetic moment it is the boundary between open and closed drift trajectories) continously shrinks up until 18:00 UT.

Plate 1

Also plotted in Plate 1 is the equivalent magnetic disturbance D_{ENA} from the proton distributions inverted from the ENA images as described above. Squares represent the individual energies as indicated and stars represent the total sum. The values of the total D_{ENA} have been scaled to fit on the same scale as SYMH and more specifically to coincide with the SYMH at 04:21 UT. We stress that our estimated D_{ENA} should not be taken as absolute but as a measure of how the energy content of ions inside L=6 varies. We discuss the implications in the Discussion section.

All ENA images in this paper are presented in an azimuthal, equidistant projection of the sky hemisphere. The dipole field lines of L-shells 4, 8 and 12 are shown for reference and the MLTs are indicated by red numbers. The coordinates in rectangular (and spherical coordinates radius, latitude and longitude) solar magnetic (SM) coordinates in units of R_E of the IMAGE spacecraft for the images in Plates 2 and 4 are the following: For 06:40 UT {-1.7, 0.6, 7.8} (8.0, 76.8°, 160.0°); 08:30 UT {-3.6, 0.9, 7.2} (8.1, 62.7°, 166.1°); 17:21 UT {-0.4, -0.1, 5.5} (5.5, 86.0°, -161.9°); and 19:30 UT {-2.5, -0.9, 6.9} (7.4, 68.7°, -160.7°). In some images a narrow band of emissions runs horizontally across the upper portions. This is the solar contamination from residual sunlight hitting the detector plates. The LOSs to this contamination usually intersects L-shells much higher

than where it can effect the magnetospheric ion distribution. All HENA images in this paper are obtained with a 10 min integration time and all MENA images with 30 min integration.

During the early main phase (when the E_y was still weak) the substorms appeared to inject plasma onto closed trajectories at 06:10 and 09:24 UT (not shown). Later in the main phase as E_y had increased to about 5 mV/m the ENA images indicated substorm injections onto open drift trajectories such as for the 12:10, 14:00 UT substorms (POLAR/IPS measurements, not shown) and the 17:30 UT substorm. Although the spacecraft was located on low latitudes on the nightside as the E_y started to decrease slowly, ENA images of the injections at 20:00 and 21:30 UT (not shown) appeared to build up a more symmetric component of the ring current gradually.

4.1. Early Main Phase

Plate 2 shows the observations at 06:40 and 08:30 UT on 4 October in the 27-39 and 60-81 keV energy range. Plate 3 shows the corresponding ion distributions obtained by the inversion method described above. We see that the injection elevated the nightside ion fluxes at L=4, but fluxes remained low on the dayside. Later in Plates 3c and 3d, the nightside fluxes have decreased while the ring current appears to have become slightly more enhanced and symmetric on L=4. According to the calculated total D_{ENA} the ring current energy content of the protons during this time did not increase as can be seen in Plate 1. This implies that the O^+ may have contributed significantly to the SYMH and ASYH. We will discuss below in the Discussion section the O^+ abundance for this period.

Plate 2

Plate 3

There were two substorms at 06:10 and 09:22 UT, which both were preceded by elevated plasma sheet fluxes beyond 8 R_E. Their behavior have been reported by *C:son Brandt et al.* [2002a]. In Plate 3a plasma sheet fluxes are low, but note that in Plate 3c plasma sheet fluxes have increased which is consistent with the overall convection continuously feeding the plasma sheet with fresh plasma.

4.2. Late Main Phase

Plate 4 shows the observed ENA images in the 27-39 and 60-81 keV range for 17:21 UT and 19:30 UT. Plate 5 shows the equatorial proton distributions inverted from the ENA images in Plate 4. According to auroral FUV images obtained by the FUV camera on board IMAGE, a substorm onset occurred at approximately 17:20 UT. At 17:30 UT an ion injection was observed around midnight at geosynchronous altitudes. We can see that there is not much change in ion flux from 17:21 UT to 19:30 UT in either energy range.

Plate 4

Plate 5

If one considers that the curvature-gradient drift period

of 70 keV protons is approximately 3 h, it is reasonable to expect that the dayside ions present at 19:30 UT are the ions from the injection at 17:30 UT. For all energies in Plate 5 there are ion fluxes extending past dusk to noon and weak signatures of ion fluxes extending out to L=8 around noon. This implies that the ions at these energies curvature-gradient drifted around to noon where they were lost through the dayside magnetopause and picked up by the magnetosheath flow. The magnetopause during this time was around 11 R_E on the dusk flank and was estimated to be inside L=8 at the subsolar point using the fits by *Roelof and Sibeck* [1993]. It is clear that there are almost no ion fluxes in the pre noon sector for 60-81 keV which implies that the drift trajectories were open at this energy. We also note that the MLT region spanned by the partial ring current leaves only a narrow sector in MLT with significantly lower ion fluxes. Thus a finite number of in-situ measurements at geosynchronous orbit could run a high risk of missing this minimum, making it look like the ring current was still closed during this time. It is also interesting to note that the 27-39 keV proton distribution at 19:30 in Plate 5c display higher intensities at L>8 on the nightside than at 17:21 UT. The reason for this may be related to the fact that a dipolarization occured around the 17:30 substorm which transported the plasmasheet ions to the inner magnetosphere. At 19:30 UT, however, the $\mathbf{E}\times\mathbf{B}$ drift from further down the tail has had time to transport fresh plasma in to the plasmasheet. This pattern can also be seen in Plates 3a and 3c.

19:30 UT is also the time of the deepest minimum of SYMH in Plate 1, but this does not seem to be reflected in the proton distributions and D_{ENA}. Again, the cause for this is most likely the contribution from O^+ or possibly a tail current contribution.

Plate 6 shows the ENA images from the MENA imager in the 1.0-5.3 keV energy range. We immediately note the similarity between these and the ones observed by HENA at 27-39 keV (Plate 4a). We have not inverted the MENA images, so the comparison has to be qualitative. The observations at MENA energies are essential since the ions are dominated by the electric drifts at these energies. From Plate 6 we see that there is perhaps a weak maximum in the post-midnight sector, and that the ENA fluxes decrease rapidly once beyond dusk. In Plates 4a and 4b we see that the ENA fluxes continue beyond dusk. This is reasonable since at higher energies the curvature-gradient drift should be more pronounced. However, the change of the morphology over the entire energy range is not drastic, and we will discuss below how this can imply significant electric field magnitudes deep in the inner magnetosphere.

Plate 6

5. DISCUSSION

In order to answer the original question about how much substorms contribute to the growth of the geomagnetic storm, consider Plates 3 and 5. The proton distributions are clearly asymmetric in MLT. This means that the substorms did not induce electric fields sufficiently strong to inject protons onto stably trapped orbits. Also, ENA images (not presented here) from POLAR/IPS at 11:30-14:30 UT show the development of another two substorms, supporting the above conclusion. The first substorm ocurred at approximately 12:10 UT and the second around 14:00 UT. Neither of these injections showed any indications of being on closed trajectories. This implies that convection responsible for increasing the energy of proton ring current during this main phase.

It is also clear from Plate 1 that the substorm injections at 17:30, 20:00, and 21:30 UT did not increase the proton ring current energy. We will discuss the O^+ content next. If we consider our calculated D_{ENA} in Plate 1 we can see that it does not decrease as much as the SYMH. At the time of these observations the mass resolving capability of HENA had not been optimized. However, we know that the $<$10 keV/nucleon hydrogen channel is dominated by $\sim$80-160 keV oxygen, which has the same velocity as $<$10 keV hydrogen. The reason for this is that the energy of a $<$10 keV/nucleon hydrogen atom is too low to penetrate the front foil of HENA.

Figures 1 and 2 show the image integrated ENA flux in the lowest energy per nucleon channel over the entire main phase. We see that the total oxygen ENA flux increases about one order of magnitude over the entire main phase. This shows that the ring current energy increased significantly in the O^+ population. Superposed on this long term increase there are intensifications at every substorm onset that decay away during an hour. This is consistent with the idea that the substorm dipolarizations energize O^+ in the plasmasheet and trap a fraction of O^+, which is reflected as the gradual increase of the oxygen ENA flux over the main phase. The decay of the oxygen ENA "bursts" can be explained as the part of the O^+ that is drifting out from the magnetosphere on open trajectories. Consequently, the more substorms, the more O^+ is added and the higher the energy of the ring current becomes. If we take the oxygen ENA fluxes at face value, the ring current energy should decrease shortly after the 17:30 UT injection until 19:30 UT when a second substorm injection appears to occur. The second injection or "burst" decays away until around 21:30 UT when a third burst appears that reaches its maximum at around 22:00 UT and then gradually decays away.

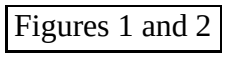

The bursts of oxygen ENAs and the lack of the same signature in the hydrogen ENAs are worth discussing. Recent modeling results by *Delcourt* [2002] show that the induced

dipolarization electric field occurs in timescales of the gyroperiod of ∼1 keV O^+, which leads to a significant diabatic energization of the O^+ up to ∼100 keV. This energization mechanism is not efficient for ∼10 keV protons. A reasonable scenario for the occurence of the oxygen bursts would therefore be one where O^+ is, more or less, continuously extracted from the ionosphere to the plasmasheet during southward IMF. The O^+ would reach about <1 keV in the plasmasheet, and at every dipolarization it would be energized up to ∼100 keV and transported to the inner magnetosphere where it would show up as bright bursts of oxygen ENA. This is a topic that is currently under deeper investigation and more results will soon appear in *Space Science Reviews*.

Comparing the oxygen ENA flux with the SYMH there is an increase at around 17:30 UT, then the SYMH decreases (ring current energy increase) until about about 19:30 when SYMH minimum is reached around which a new SYMH increase is seen. Then, again, shortly after 21:00 UT there is a new SYMH increase. In summary, it seems almost as if the oxygen ENA bursts track the SYMH, which is inconsistent if the SYMH was only measuring the energy content of the ring current. We think the explanation for the inconsistency is that at substorm onset the magnetic signature of the disruption of the tail current is strong enough to cause an increase of the SYMH as was discussed by *Ohtani et al.* [2001]. It is not our intention to fully explore that here, but rather outline as a possibility.

At this stage we can only say that we would expect a significant long term contribution of the O^+ ions because of the one order of magnitude increase in oxygen ENA flux. So, in this sense substorms appear to play an important role in the long term increase of the O^+ energy content in the magnetosphere. ENA image inversion at these energies is difficult to interpret in detail due to a larger angular scattering (up to 20°) in the front foil.

A natural question arising is why the injections at 12:10, 14:00 (POLAR/IPS ENA images) and 17:30 UT (Plate 5) did not become trapped. At first glance the substorm induced electric field should decrease the size of the Alfven boundary, and that same field would transport particles to its boundary. As the induced electric field decreased, the Alfven boundary then would be expected to increase rapidly and leave the particles inside it, thus placing them on closed drift paths. This simple scenario is valid only if the shielding of the electric field was constant in time. In fact under shielding is expected to occur during substorms. If the shielding decreases during the substorm and the lower values of the shielding are maintained (even after the injection is complete), the Alfven layer will stay at the smaller size, allowing ions to still drift on open trajectories.

Another interesting scenario can be realized if one con-

siders the fact that there exist significant electric fields up to 6 mV/m between L=2 and L=4 [*Wygant et al.*, 1998]. The electric drift velocity in such high electric fields at L=4 would be comparable to the gradient-curvature drift of $\leq$100 keV ions. This means that $\leq$100 keV ions injected onto L$<$4 would experience electric as well as magnetic drifts and may not become trapped. It is therefore relevant to briefly discuss the implications of the electric field pattern that can be inferred from our observations. Consider the pattern of the ion distribution during the later main phase in Plate 5 and Plate 6. The intense ion fluxes around midnight and L=3 are persistent features for all energies 1-200 keV. According to the POLAR/IPS observation, it appears this feature had been reasonably stable over the 14:00-22:00 UT period.

In the 1.0-5.3 keV range the motion of the ions is dominated by electric drifts. Therefore important implications can be made by studying the ENA images in this energy range (Plate 6). In the superposition of a pure dawn to dusk electric field plus a corotation electric field, the electric drifts would carry the low energy ions straight through on the dawn side. Inspecting Plate 6, it appears that the electric field is configured such that ions will be deflected both at dawn and dusk.

From inspection of the higher energies in Plates 5a and 5b, it is evident that ions have succeeded in drifting to the dayside, but they have decreased in flux considerably. This implies that the high energy ions either (1) are being deviated from their curvature-gradient drift trajectories and are lost through the magnetopause in the post-noon sector, (2) decrease their energy so that their differential flux decreases at a given energy, or a combination of these two.

In conclusion we can say that there must have been a strong enough field to first bring the ions in to L=3 and that the electric field there changed dramatically to have no, or a very small, positive y-component that would otherwise allow low energy ions to drift across the dawn to dusk meridian, or perhaps the electric field is twisted as a function of radial distance. The implications for strong electric fields in the inner magnetosphere has been discussed and reported by *C:son Brandt et al.* [2002b].

We would like to draw attention to a study by *Ridley and Liemohn* [2002] where they estimated the inner magnetospheric electric field that is set up by the asymmetric ring current. Using the kinetic ring current model by *Liemohn et al.* [2001] they calculated the electric field pattern in the ionosphere due to the region 2 currents of the asymmetric ring current. The ionospheric potential was then mapped back out to the equatorial plane assuming the magnetic field lines to be infinitely conducting. They found strong electric fields inside L=3 with strong eastward and outward radial components in the post-midnight sector and equally

strong westward and outward radial components in the pre-midnight sector (see their Plate 2). Superposed on this was also the over all dawn to dusk field and corotational field. This would stretch their patterns slightly more towards dusk. Such strong electric field on low L-shells have been reported by *Wygant et al.* [1998]. This type of self-consistent modeling was pioneered by [*Wolf*, 1983] in their Rice Convection Model (RCM) who also noticed the same type of westward skewing that we have observed. *Fok et al.* [2001] has succesfully coupled a kinetic ring current model with the RCM. About three different storm observations has been compared to runs of this model with a very good agreement.

Low energy ions drifting in such an electric field would therefore drift eastward and then inward until they come closer to the Earth near dawn where the outward pointing electric field would transport them westward past local midnight. As the low energy ions reach dusk the eastward electric field component would cause the ions to drift outward and be lost through the duskside/afternoon magnetopause. This general pattern is consistent with our observations.

At high energies ions will start to curvature-gradient drift strongly once they are convected into L=3. As they drift around towards dusk our observations show that they decrease their intensity drastically. However, there are still weak ion fluxes close to noon, as can be seen in Plates 5a and 5b. At these energies the dominating transport is most likely curvature-gradient drift, but our observations imply that there is indeed a significant electric field such that even the high energy ions may be lost through the dusk to afternoon magnetopause. Without detailed kinetic modeling it is difficult to answer how much of the flux decrease is due to transport to weaker magnetic field strength, and how much can be attributed to loss through the magnetopause.

Although the electric field pattern obtained by *Ridley and Liemohn* [2002] qualitatively agrees with our observations, it does not answer how the ions were transported inward to L=3 in the first place. The dawn to dusk electric field during 4 October was $\leq$5 mV/m which is not extreme by any means, but may have been sufficient to transport the ions all the way in to L$\leq$3 where the electric field driven by the asymmetric ring current would take over.

6. Summary and conclusions

We have presented the global equatorial proton distributions in the 16-198 keV energy range for the main phase of the 4 October 2000. The proton distributions were obtained by applying a constrained linear inversion technique [*Twomey*, 1977] to ENA images observed by IMAGE/HENA. The IMF B_z decreased steadily from early on the 4 October and slowly started to increase again around 19:00 UT. During the entire 4 October about a half a dozen substorms

occurred with regular intervals of which two were described in this paper. In the early main phase, when the dawn to dusk electric field was still weak, the substorm appeared to inject ions onto closed trajectories. When E_y increased in strength, substorms injected particles onto open trajectories. As E_y started to slowly decrease at around 19:00 UT, substorm injections appeared to become trapped.

Up to the time of minimum SYMH we found that no significant symmetric component of the proton ring current had developed, which implies that substorms did not build up a durably trapped proton population and therefore did not contribute directly to the long term energy increase of the main-phase ring current. Also, from the time of E_y=0 to the time of maximum E_y the peak ring current moved in from L=5 to L=3. This is consistent with the increase in E_y which decreases the size of the Alfven boundary. In this respect the increase in solar wind driven convection is the long term contributor to increased energy content of the (partial) proton ring current.

In order to estimate the contribution to the energy content of the ring current from the obtained proton distributions we calculated the equivalent magnetic disturbance (D_{ENA}) at the Earth's surface at the equator using the DPS relation [*Dessler and Parker*, 1959; *Sckopke*, 1966] for the L$\leq$6 proton distributions. The D_{ENA} was calculated for the 16-198 keV energy range in seven energy bins as indicated in Plate 1. We found that our proton distributions did not fully account for the SYMH depression. We expect that the O^+ will contribute significantly to the SYMH. Some contribution from enhanced tail currents may also have to be considered.

A preliminary inspection of the $\sim$80-160 keV oxygen ENA fluxes revealed a one order of magnitude gradual increase over the entire main phase, which we expect would have a significant contribution to the ring current energy build up. Superimposed on the gradual increase, oxygen ENA fluxes displayed $\sim$1 h increases and decreases starting at every substorm onset. This is consistent with low-energy ionospheric O^+ in the plasma sheet being energized up to $\sim$100 keV during each substorm dipolarization [*Delcourt*, 2002]. The observed gradual increase of oxygen ENA during the main phase is consistent with the idea that O^+ is being trapped. In this respect, substorms contributed to the long term ring current energization.

The fact that the substorm around 17:30 UT injected protons onto open trajectories (with very little change to the asymmetric ring current pattern), raises the question of whether strong electric fields were present at L$<$4. We discussed studies by *Wygant et al.* [1998] and *Ridley and Liemohn* [2002] and found that our observations were consistent with their conclusions and observations of 5-10 mV/m electric

fields in the inner region L<4.

Acknowledgments. Thanks to M. W. Liemohn, University of Michigan and A. T. Y. Lui at the Johns Hopkins University Applied Physics Laboratory, Maryland for stimulating discussions. Thanks also to Dominique Delcourt, Centre National de la Recherche Scientique, France, for modeling results of the response of O^+ to substorms.

REFERENCES

Akasofu, S. I., *Polar and magnetospheric substorms*, D. Reidel, Norwell, Mass., 1968.

C:son Brandt, P., S. Barabash, E. C. Roelof, and C. J. Chase, ENA imaging at low altitudes from the Swedish microsatellite Astrid: Extraction of the equatorial ion distribution, *J. Geophys. Res.*, *106*, 25,731–25,744, 2001.

C:son Brandt, P., R. Demajistre, E. C. Roelof, D. G. Mitchell, and S. Mende, IMAGE/HENA: Global ENA imaging of the plasmasheet and ring current during substorms, *J. Geophys. Res.*, 2002a, in press.

C:son Brandt, P., S. Ohtani, D. G. Mitchell, M. C. Fok, E. C. Roelof, and R. Demajistre, Global ena observations of the storm mainphase ring current: Implications for skewed electric fields in the inner magnetosphere, *Geophys. Res. Lett.*, 2002b, in press.

Delcourt, D. C., Particle acceleration by inductive electric fields in the inner magnetosphere, *J. of Atmosph. and Solar-Terr. Phys.*, *64*, 551–559, 2002.

Dessler, A. J., and E. N. Parker, Hydromagnetic theory of geomagnetic storms, *J. Geophys. Res.*, *64*, 2239–2252, 1959.

Fok, M. C., R. A. Wolf, R. W. Spiro, and T. E. Moore, Comprehensive computational model of Earth's ring current, *J. Geophys. Res.*, *106*, 8417–8424, 2001.

Gonzalez, W. D., and B. T. Tsurutani, Criteria of interplanetary parameters causing intense magnetic storms (D_{st} <-100 nt), *Planetary and Space Sci.*, *35*, 1101, 1987.

Henderson, M. G., G. D. Reeves, H. E. Spence, R. B. Sheldon, A. M. Jorgensen, J. B. Blake, and J. F. Fennell, First energetic neutral atom images from polar, *Geophys. Res. Lett.*, *24*, 1167–1170, 1997.

Liemohn, M. W., J. U. Kozyra, M. F. Thomsen, J. L. Roeder, G. Lu, J. E. Borovsky, and T. E. Cayton, The dominant role of the asymmetric ring current in producing the stormtime Dst, *J. Geophys. Res.*, *106*, 10,883–10,904, 2001.

Ohtani, S., M. Nose, G. Rostoker, H. Singer, A. T. Y. Lui, and M. Nakamura, Storm-substorm relationship: Contribution of the tail current to dst, *J. Geophys. Res.*, *106*, 21,199–21,209, 2001.

Perez, J. D., G. Kozlowski, P. C. Brandt, D. G. MItchell, J. M. Jahn, C. J. Pollock, and X. Zhang, Initial ion equatorial pitch angle distributions from energetic netural atom images obtained by IMAGE, *Geophys. Res. Lett.*, *28*, 1155–1158, 2001.

Rairden, R. L., L. A. Frank, and J. D. Craven, Geocoronal imaging with dynamics explorer, *J. Geophys. Res.*, *91*, 13,613–13,630, 1986.

Ridley, A. J., and M. W. Liemohn, A model-derived stormtime asymmetric ring current driven electric field description, *J. Geophys. Res.*, 2002, acce,pted Aug 2001.

Roelof, E. C., and D. G. Sibeck, Magnetopause shape as a bivariate function of interplanetary magnetic field B_z and solar wind dynamic pressure, *J. Geophys. Res.*, *98*, 21,421–21,450, 1993.

Roelof, E. C., and A. J. Skinner, Extraction of ion distributions from magnetospheric ENA and EUV images, *Space Sci. Rev.*, *91*, 437–459, 2000.

Sckopke, N., A general relation between the energy of trapped particles and the disturbance field near the Earth, *J. Geophys. Res.*, *71*, 3125–3130, 1966.

Twomey, S., *Introduction to the mathematics in remote sensing and indirect measurements*, Developments in geomathematics 3, 1st ed., Elsevier scientific publishing company, 1977.

Wolf, R., *Solar Terrestrial Physics*, pp. 303–368, D. Reidel, Hingham, MA, 1983.

Wygant, J., D. Rowland, H. J. Singer, M. Temerin, F. Mozer, and M. K. Hudson, Experimental evidence on the role of the large spatial scale electric field in creating the ring current, *J. Geophys. Res.*, *103*, 29,527–29,544, 1998.

Plate 1. The SYM-H (black line) and the negative of the ASY-H index (green line) and the IMF E_y during the early main phase. Squares represent the differential energy contribution to the ring current as indicated by the color coding and stars represents the total energy contribution (see section 3).

Plate 1. The SYM-H (black line) and the negative of the ASY-H index (green line) and the IMF E_y during the early main phase. Squares represent the differential energy contribution to the ring current as indicated by the color coding and stars represents the total energy contribution (see section 3).

Plate 2. The first substorm injection during the early main phase occurred at 06:10 UT. This plate shows the hydrogen ENA images 30 min and 140 min after the injection. The ENA image at (a) 06:40 UT at 27-39 keV, (b) 06:40 UT at 60-81 keV (c) 08:30 UT at 27-39 keV, and (d) 08:30 UT at 60-81 keV. Note that the ENA flux decreases although the ASYMH increases.

Plate 2. The first substorm injection during the early main phase occurred at 06:10 UT. This plate shows the hydrogen ENA images 30 min and 140 min after the injection. The ENA image at (a) 06:40 UT at 27-39 keV, (b) 06:40 UT at 60-81 keV (c) 08:30 UT at 27-39 keV, and (d) 08:30 UT at 60-81 keV. Note that the ENA flux decreases although the ASYMH increases.

Plate 3. The proton fluxes obtained from the inversions of Plate 2 plotted in the equatorial plane. Only the isotropic pitch angle component is shown. (a) 06:40 UT and 27-39 keV. The injection is clearly visible on the nightside. A minimum appears in the pre noon sector. (b) 06:40 UT and 60-81 keV. Intensities lower but pattern almost unchanged. (c) 08:30 UT and 27-39 keV. High intensities on the nightside are still visible. Ion distribution appears more isotropic. (d) 08:30 UT and 60-81 keV. Weak maximum appears on nightside and around noon.

Plate 3. The proton fluxes obtained from the inversions of Plate 2 plotted in the equatorial plane. Only the isotropic pitch angle component is shown. (a) 06:40 UT and 27-39 keV. The injection is clearly visible on the nightside. A minimum appears in the pre noon sector. (b) 06:40 UT and 60-81 keV. Intensities lower but pattern almost unchanged. (c) 08:30 UT and 27-39 keV. High intensities on the nightside are still visible. Ion distribution appears more isotropic. (d) 08:30 UT and 60-81 keV. Weak maximum appears on nightside and around noon.

Plate 4. Observed hydrogen ENA images from (a) 17:21 UT and 27-39 keV, (b) 17:21 UT and 60-81 keV, (c) 19:30 UT and 27-39 keV, and (d) 19:30 UT and 60-81 keV.

Plate 4. Observed hydrogen ENA images from (a) 17:21 UT and 27-39 keV, (b) 17:21 UT and 60-81 keV, (c) 19:30 UT and 27-39 keV, and (d) 19:30 UT and 60-81 keV.

Plate 5. Equatorial ion distributions inverted from the ENA images in Plate 4.

Plate 5. Equatorial ion distributions inverted from the ENA images in Plate 4.

Plate 6. MENA images obtained in the (a) 1.0-2.3 keV range and (b) 2.3-5.3 keV range. The morphology is quite similar to that obtained by HENA in the higher energy range. See Plates 4a and 4b, but note the different colorbar.

Plate 6. MENA images obtained in the (a) 1.0-2.3 keV range and (b) 2.3-5.3 keV range. The morphology is quite similar to that obtained by HENA in the higher energy range. See Plates 4a and 4b, but note the different colorbar.

Figure 1. The integrated oxygen ENA flux in the ∼80-160 keV range over the first half of the main phase.

Figure 1. The integrated oxygen ENA flux in the ∼80-160 keV range over the first half of the main phase.

Figure 2. The integrated oxygen ENA flux in the ∼80-160 keV range over the second half of the main phase.

Figure 2. The integrated oxygen ENA flux in the ∼80-160 keV range over the second half of the main phase.

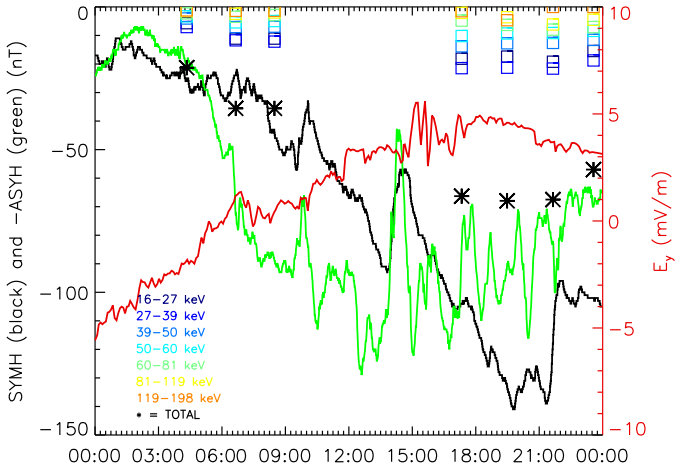
SYMH (black) and −ASYH (green) (nT)
0
−50
−100
−150
10
5
0
−5
−10
E_y (mV/m)
16−27 keV
27−39 keV
39−50 keV
50−60 keV
60−81 keV
81−119 keV
119−198 keV
• = TOTAL
00:00 03:00 06:00 09:00 12:00 15:00 18:00 21:00 00:00

PLATE 1

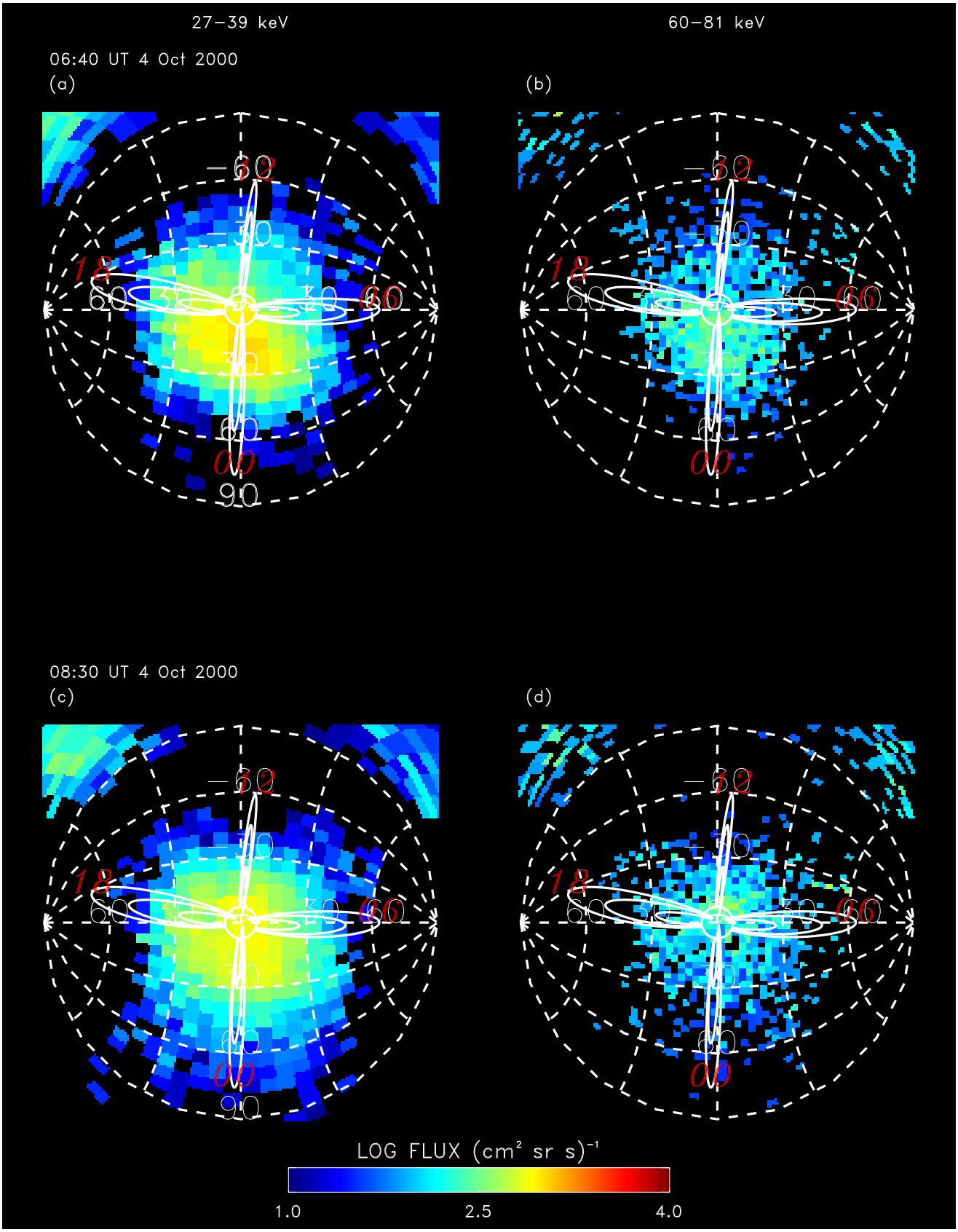
27–39 keV
60–81 keV
06:40 UT 4 Oct 2000
(a)
(b)
08:30 UT 4 Oct 2000
(c)
(d)
LOG FLUX (cm² sr s)⁻¹
1.0
2.5
4.0

PLATE 2

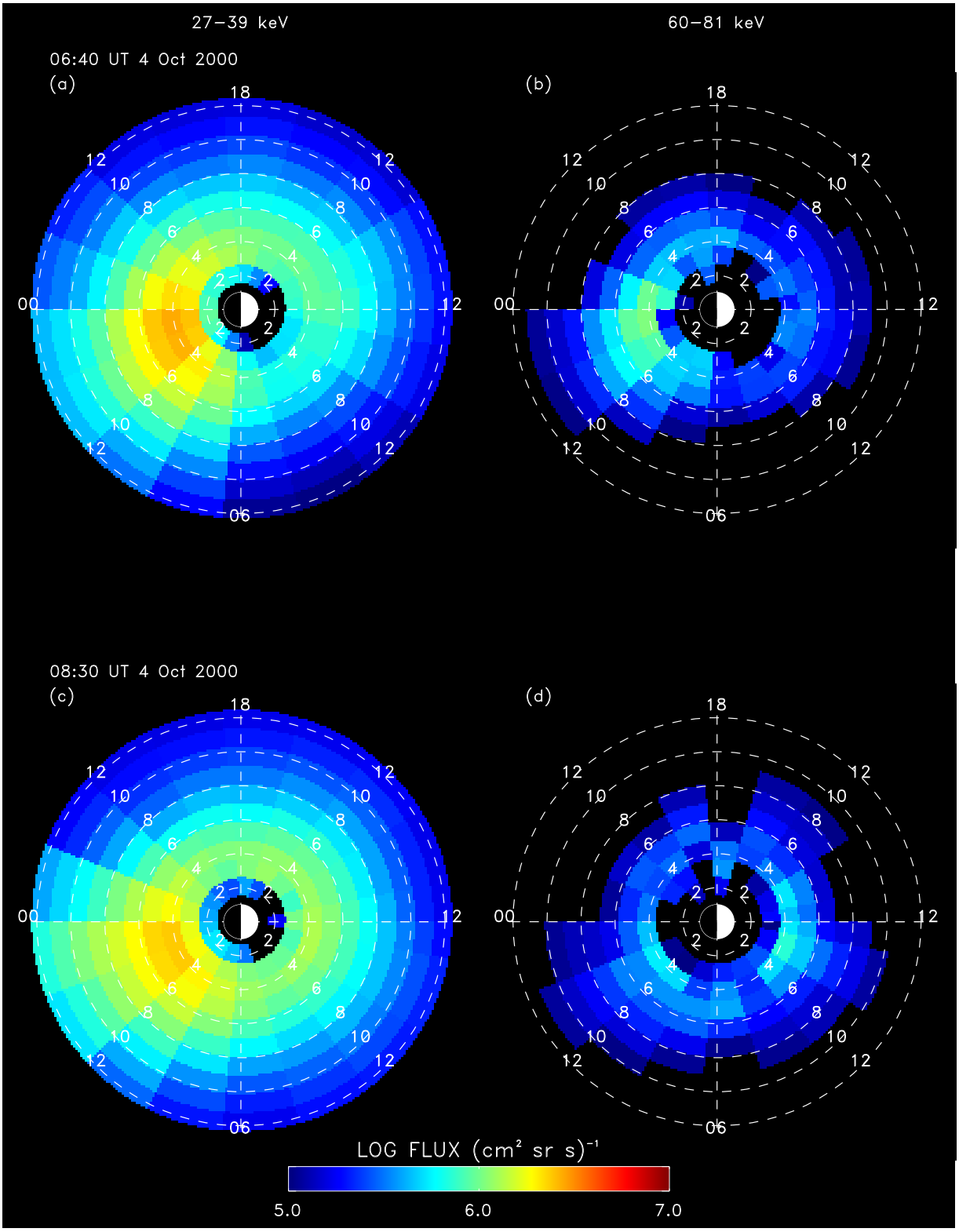
27–39 keV
60–81 keV
06:40 UT 4 Oct 2000
(a)
(b)
08:30 UT 4 Oct 2000
(c)
(d)
LOG FLUX (cm² sr s)⁻¹
5.0
6.0
7.0

PLATE 3

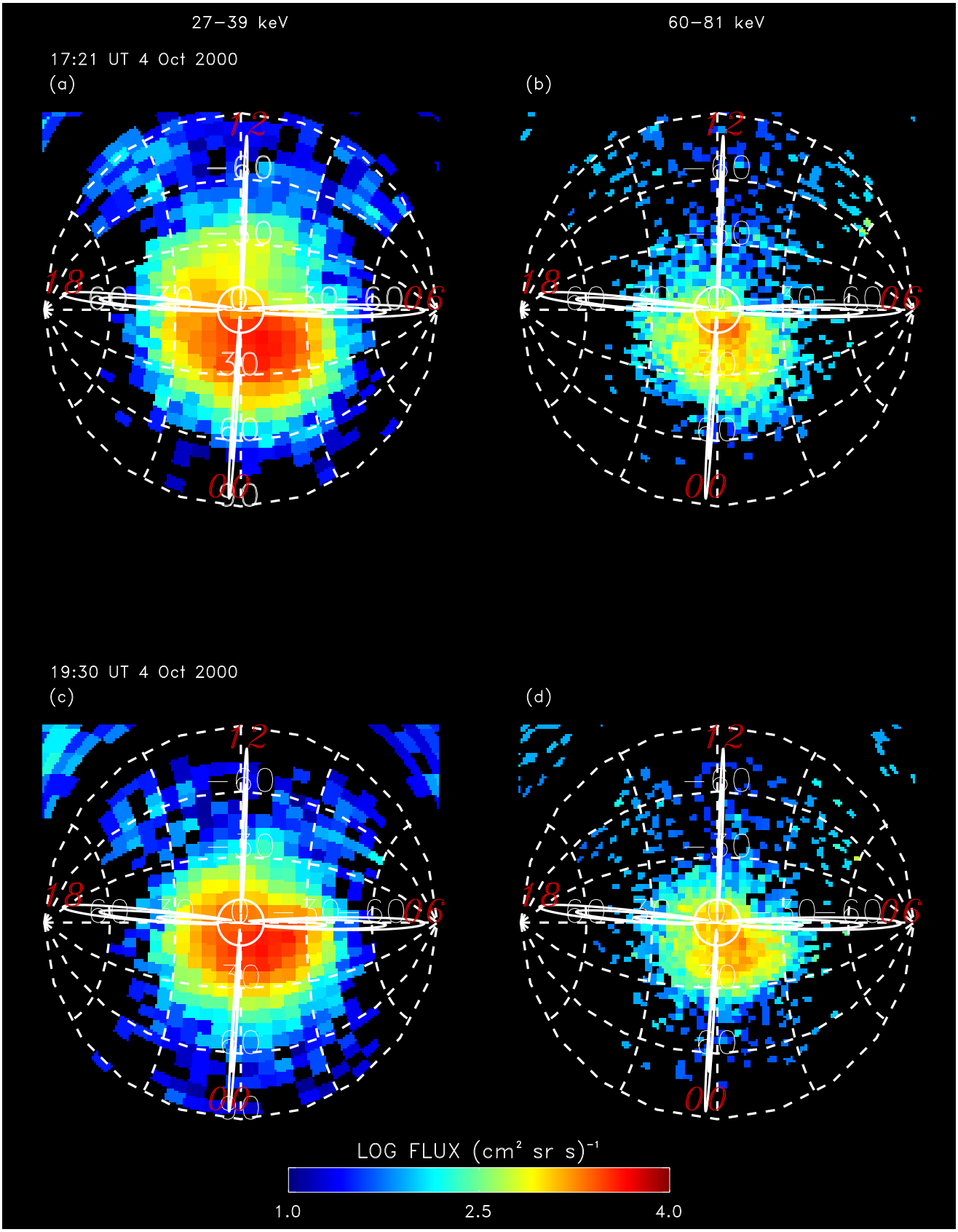
27–39 keV
60–81 keV
17:21 UT 4 Oct 2000
(a)
(b)
19:30 UT 4 Oct 2000
(c)
(d)
12
18
06
00
60
30
0
LOG FLUX (cm² sr s)⁻¹
1.0
2.5
4.0

PLATE 4

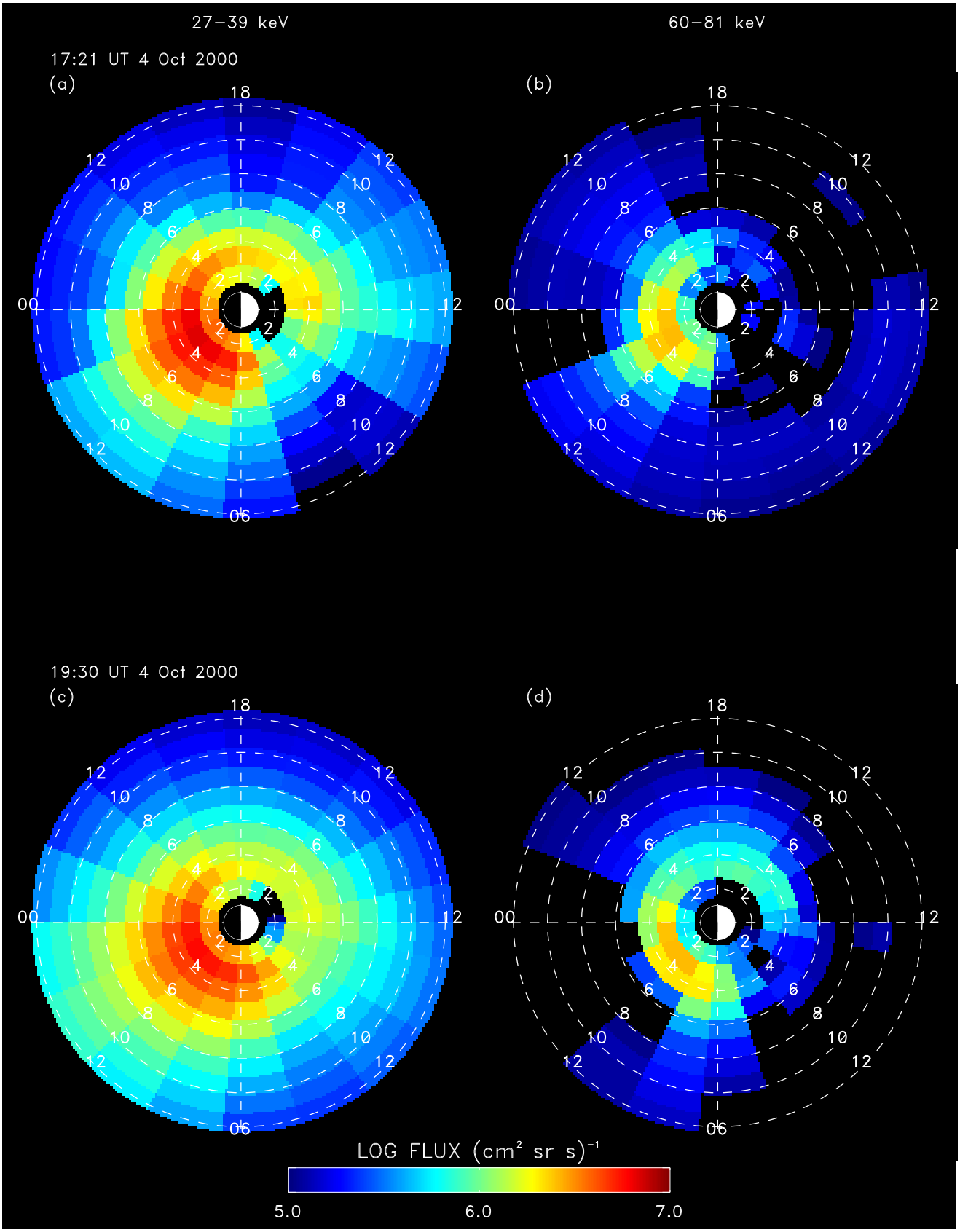
27–39 keV
60–81 keV
17:21 UT 4 Oct 2000
(a)
(b)
19:30 UT 4 Oct 2000
(c)
(d)
18
12
10
8
6
4
2
00
06
LOG FLUX (cm² sr s)⁻¹
5.0
6.0
7.0

PLATE 5

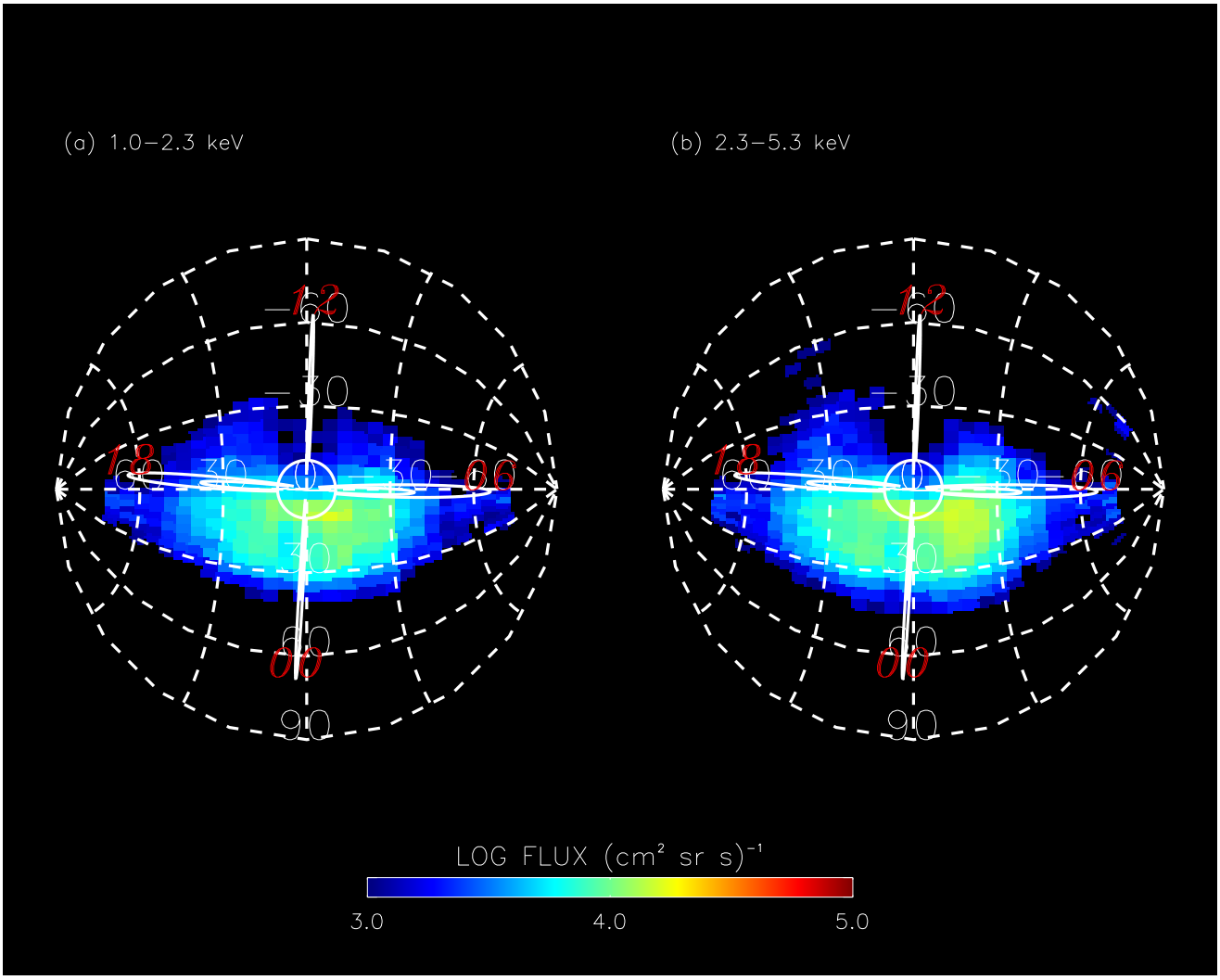

PLATE 6

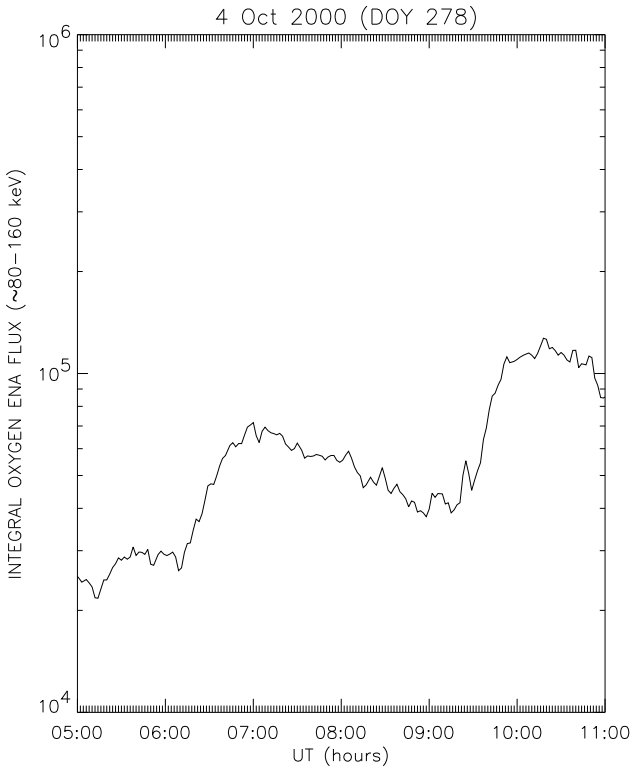
4 Oct 2000 (DOY 278)
INTEGRAL OXYGEN ENA FLUX (~80–160 keV)
10^6
10^5
10^4
05:00
06:00
07:00
08:00
09:00
10:00
11:00
UT (hours)

FIGURE 1

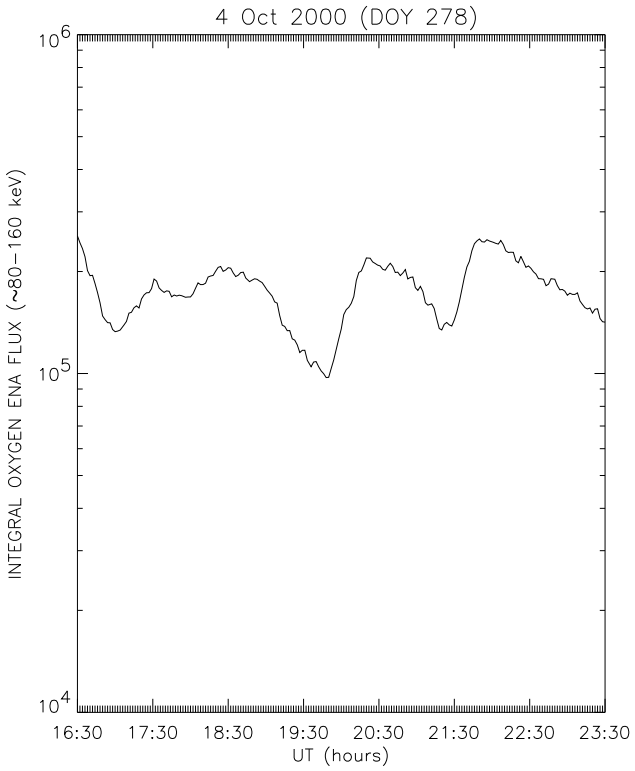
4 Oct 2000 (DOY 278)
INTEGRAL OXYGEN ENA FLUX (~80–160 keV)
10^6
10^5
10^4
16:30
17:30
18:30
19:30
20:30
21:30
22:30
23:30
UT (hours)

FIGURE 2

STORM-SUBSTORM RELATIONSHIPS OF 4 OCT STORM

C:SON BRANDT ET AL.

STORM-SUBSTORM RELATIONSHIPS OF 4 OCT STORM

C:SON BRANDT ET AL.

STORM-SUBSTORM RELATIONSHIPS OF 4 OCT STORM

C:SON BRANDT ET AL.

STORM-SUBSTORM RELATIONSHIPS OF 4 OCT STORM

C:SON BRANDT ET AL.

STORM-SUBSTORM RELATIONSHIPS OF 4 OCT STORM

C:SON BRANDT ET AL.

STORM-SUBSTORM RELATIONSHIPS OF 4 OCT STORM

C:SON BRANDT ET AL.

STORM-SUBSTORM RELATIONSHIPS OF 4 OCT STORM

C:SON BRANDT ET AL.

STORM-SUBSTORM RELATIONSHIPS OF 4 OCT STORM

C:SON BRANDT ET AL.

STORM-SUBSTORM RELATIONSHIPS OF 4 OCT STORM

C:SON BRANDT ET AL.

STORM-SUBSTORM RELATIONSHIPS OF 4 OCT STORM

C:SON BRANDT ET AL.

STORM-SUBSTORM RELATIONSHIPS OF 4 OCT STORM

C:SON BRANDT ET AL.

STORM-SUBSTORM RELATIONSHIPS OF 4 OCT STORM

C:SON BRANDT ET AL.

STORM-SUBSTORM RELATIONSHIPS OF 4 OCT STORM

C:SON BRANDT ET AL.

STORM-SUBSTORM RELATIONSHIPS OF 4 OCT STORM

C:SON BRANDT ET AL.

STORM-SUBSTORM RELATIONSHIPS OF 4 OCT STORM

C:SON BRANDT ET AL.

STORM-SUBSTORM RELATIONSHIPS OF 4 OCT STORM

C:SON BRANDT ET AL.

STORM-SUBSTORM RELATIONSHIPS OF 4 OCT STORM

C:SON BRANDT ET AL.

STORM-SUBSTORM RELATIONSHIPS OF 4 OCT STORM

C:SON BRANDT ET AL.

STORM-SUBSTORM RELATIONSHIPS OF 4 OCT STORM

C:SON BRANDT ET AL.

STORM-SUBSTORM RELATIONSHIPS OF 4 OCT STORM

C:SON BRANDT ET AL.

STORM-SUBSTORM RELATIONSHIPS OF 4 OCT STORM

C:SON BRANDT ET AL.

STORM-SUBSTORM RELATIONSHIPS OF 4 OCT STORM

C:SON BRANDT ET AL.

STORM-SUBSTORM RELATIONSHIPS OF 4 OCT STORM

C:SON BRANDT ET AL.

STORM-SUBSTORM RELATIONSHIPS OF 4 OCT STORM

C:SON BRANDT ET AL.

STORM-SUBSTORM RELATIONSHIPS OF 4 OCT STORM

C:SON BRANDT ET AL.

STORM-SUBSTORM RELATIONSHIPS OF 4 OCT STORM

C:SON BRANDT ET AL.

STORM-SUBSTORM RELATIONSHIPS OF 4 OCT STORM

C:SON BRANDT ET AL.

STORM-SUBSTORM RELATIONSHIPS OF 4 OCT STORM

C:SON BRANDT ET AL.